Int. J. Electrochem. Sci., 15 **(2020)** 3089 – 3103, doi: 10.20964/2020.04.41

International Journal of ELECTROCHEMICAL SCIENCE
www.electrochemsci.org

High-stable Phosphorene-supported Bimetallic Pt-Pd Nanoelectrocatalyst for *p*-Aminophenol, β-Galactosidase, and *Escherichia coli*

Zhentao Li[1,2], Yanhui Fu[1], Qingsheng Zhu[1], Saijin Wei[1,], Jie Gao[1,2], Yifu Zhu[2], Ting Xue[2], Ling Bai[2], Yangping Wen[2,3,*]*

[1] Institute of Applied Microbiology, College of Biological Science and Engineering, Jiangxi Agricultural University, Nanchang 330045, PR China
[2] Institute of Functional Materials and Agricultural Applied Chemistry, Jiangxi Agricultural University, Nanchang 330045, PR China
[3] Key Laboratory of Crop Physiology, Ecology and Genetic Breeding, Ministry of Education, Jiangxi Agricultural University, Nanchang 330045, P. R. China.
[*]E-mail: weisaijin@126.com (S. Wei), wenyangping1980@jxau.edu.cn (Y. Wen)

Received: 8 December 2019 / *Accepted:* 29 Januaary 2020 / *Published:* 10 March 2020

Phosphorene (BP) is a rapidly rising star in two-dimensional (2D) layered nanomaterials beyond graphene, and its urgent issues of ambient instability still have to be resolved. Here, the bimetallic Pt-Pd nanoparticle on the BP surface was employed as multifunctional chemical and biochemical sensing platform for electrocatalytic detection of *p*-aminophenol (PAP), β-galactosidase (β-Gal), and *Escherichia coli* (*E. coli*). The BP-supported Pt-Pd nanoelectrocatalyst obtained by the electrodeposition of bimetallic Pt-Pd nanoparticle onto the BP surface was very stable in aqueous buffer containing oxygen, which displayed good voltammetric responses for PAP in a linear range of 0.02 - 5 μmol·L^{-1} with a detection limit (LOD) of 1.41 × 10^{-8} M and sensitivity 115.81 μA·μM^{-1}·cm^{-2}. PAP could be obtained by the biochemical reaction of β-Gal in the presence of substrate PAP-β-galactopyranoside, which could realize for biochemical sensing of β-Gal in a linear range of 0.2 - 0.8 mU·L^{-1} with a LOD of 9.35 nU·L^{-1} and sensitivity of 4.77 μA (mU·L^{-1})$^{-1}$·cm^{-2}. The β-Gal is an indicator of total coliforms represented by *E. coli* that are induced by isopropyl-β-thiogalactopyranoside, which could applied for biochemical sensing of *E. coli* in a linear range of 6 × 10^6 – 1.6 × 10^8 cfu·mL^{-1} with LOD of 6.65 × 10^5 cfu·mL^{-1} and sensitivity of 2.44 μA·(cfu·mL^{-1})$^{-1}$·cm^{-2}. This work will provide experimental support for multifunctional chemical and biochemical sensing platform based on 2D layered nanomaterials decorated with bimetallic nanoelectrocatalysts.

Keywords: Phosphorene; Bimetallic nanoparticles; *Escherichia coli*; β-Galactosidase; *p*-aminophenol.

1. INTRODUCTION

Phosphorene (BP), a two-dimensional (2D) layered black phosphorus nanosheet beyond graphene, has emerged as rapidly rising stars in the field of graphene-like new nanomaterials with various applications since the advent in early 2014 [1]. More fascinatingly, BP exhibits a distinctive wrinkled structure with the high hole mobility, excellent mechanical properties, tunable band structures, good electrical properties, extraordinary specific surface area, excellent biocompatibility, which led to its marvelous prospects for electronic applications in various devices [2]. However, BP has weak environmental stability and electrocatalytic capacity in an oxygenated water system [3], which effects its chemical structure and electronic properties, further led to few electrochemical applications in chemical and biochemical (chemo/bio) sensors [4-6]. Our group improved the environmental stability of BP in water containing oxygen via the surface modification strategy using different materials, which were employed for electrochemical sensing of different targets in field of agricultural analysis [7-11].

Nanoparticles (NPs) of noble metals are promising electrode materials in the field of electrocatalysis and electroanalysis because of their excellent electrocatalytic properties [12]. Bimetallic NPs consisting of two noble metals have aroused great interest their unique electronic and electrocatalytic properties far superior to their corresponding monometallic counterparts [13], especially Pt-based bimetallic nanoparticles exhibited enhanced electrocatalytic performance in both activity and selectivity because of the positive synergistic effects [14, 15]. Pt nanocatalysts by forming bimetallic nanoparticles with Pd as electrocatalysts for various applications with enhanced performance relative to their monometallic counterparts [16]. The nanocomposites of bimetallic NPs prepared by supporting them on the organic or inorganic counterparts demonstrated as an efficient way to promote the dispersion of metal active sites, and to prevent active sites from aggregation during electrocatalytic reaction processes [17]. Bimetallic nanoparticles with graphene-supported [18], carbon nanotube-supported [19, 20] show strong electrocatalytic oxidation activities and superior enzyme-like characteristics, which was widely employed in electrocatalytic fields such as fuel cells and electrochemical sensors. However, bimetallic nanoparticles with graphene analogues-supported, especially bimetallic nanoparticles with BP-supported were rarely studied.

Escherichia coli (*E. coli*), the most common gram-negative bacterium in intestines of human beings and other warm-blooded animals, is an indicator of fecal pollution generally in insanitary conditions of water, food, milk and other dairy products. *E. coli* enters the body along with water sources and other routes, invades normal intestinal flora, then causes a variety of diseases such as diarrhea, urinary tract infection, sepsis and neonatal meningitis [21, 22]. Traditional microbiological detection includes plate counting, filter membrane, and multi-tube fermentation [23]. Although these methods are very accurate, they are complex and time-consuming (more than 24 hours). Therefore, it is very necessary to develop a rapid and sensitive method for current diagnosis of pollution sources containing *E. coli* in food, water and environment.

Electrochemical chemo/biosensors as one of new methods have received increasing attention because of their simple, low-cost, fast and efficient analysis. Different electroanalytical method like amperometry, voltammetry, impedance methods were selected for developing amperometric sensors

and impedimetric sensors [24], but voltammetric sensors [25] as one of sensitive methods have been rarely reported. Different biological recognition elements such as DNA/RNA, biological enzymes, antigens/antibodies, aptamers, and cells were developed for fabricating DNA sensors [26], enzyme sensors [27], immunosensor [28], and others [29], but only a few studies were reported on chemical sensors combined with biochemical reaction chains that avoided biosensing deficiencies like the effect of non-native environments on the lifetime. Different materials, especially nanomaterials, including conducting polymers [30], nanometal and their oxides [31] carbon nanomaterials [32] and nanocomposites/nanohybrids [33] was employed as electrode modified materials of chemically modified electrode, but there are very few reports on graphene-like new materials as electrode modified materials of chemically modified electrode.

Here, we reported a high-stable BP-supported bimetallic Pt-Pd nanoelectrocatalyst for chemo/biosensing of PAP, β-Gal and *E. coli* (Scheme 1). Morphology ambient stability and electrochemical properties of bimetallic Pt-Pd nanoparticles-modified BP was characterized, then the multifunctional chemo/biosensing application of the BP nanocomposite electrode were studied, which allows the development of a multifunctiomal chemical and biochemical sensing platform.

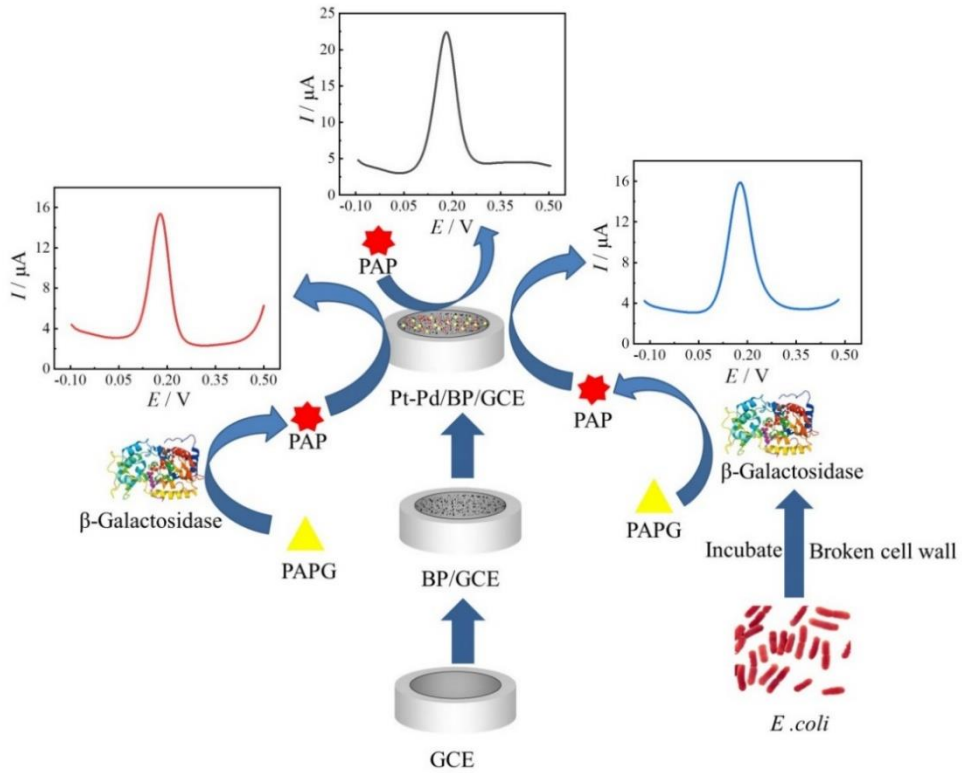

Scheme 1. Bimetallic Pt-Pd nanoparticles decorated BP as nanoelectrocatalyst for electrochemical application in chemical and biochemical sensing of PAP, β-Gal, and *Escherichia coli*.

2. EXPERIMENTAL

2.1 Chemicals

BP (0.2 mg/ml) was purchased from XFNANO Materials Tech Co., Ltd (Nanjing, China).

Chloroplatinic acid was obtained from Adamas Reagent Co., Ltd. (Shanghai, China). Potassium chloropalladite and *p*-aminophenol (PAP) were purchased from Aladdin Reagent Co. Ltd. (Shanghai, China). β-Gal, Polymyxin B Sulfate (POL-BS) and lysozyme (LYS) were received from Solarbio Technology (Beijing, China). *p*-aminophenyl-β-D-galactopyranoside (PAPG) was bought from TCI (Shanghai) Development Co., Ltd. (Shanghai, China). *E. coli* (BL21) was obtained from College of Bioscience and Bioengineering in Jiangxi Agricultural University (Jiangxi, China). Luria broth medium was made up from 1.0% tryptone, 0.5% sodium chloride and 0.5% yeast extract. All solutions were prepared with doubly distilled water.

2.2 Apparatus

Scanning electron microscopy (SEM) was conducted with a Quanta 250 microscope (FEI Company, The United States). Electrochemical measurements were performed on a CHI 660E electrochemical workstation (CH Instruments, Chenhua, Shanghai, China) with a three-electrode system consisting of an Ag/AgCl/3.0 M KCl as the reference electrode, a platinum wire electrode as the auxiliary electrode and a modified or bare glassy carbon electrode (GCE) as the working electrode.

2.3 Culture and treatment of E. coli

Scheme 2 demonstrated the cultivation and treatment of *E. coli* as well as the release of β-Gal. *E. coli* were administered in LB medium and cultured at shaker (37 ºC, 220 rpm). Five hours later, *E. coli* cultures were diluted to 1.0×10^6 and 1.0×10^8 cfu/ml in 50 mL LB medium containing 0.5 mM IPTG, and incubated for 3 h with 30 ºC, 220 rpm. The incubated *E. coli* culture medium were filtered with 0.45 μm filter membrane. Then the filter membrane was put into 25 ml PBS (pH 6.0), which include 15 μg/mL POL-BS and 25 μg/mL LYS. The PBS were shaked violently for 25 minutes with 30 ºC. Finally, PBS containing *E. coli* and its by-products β-Gal was obtained.

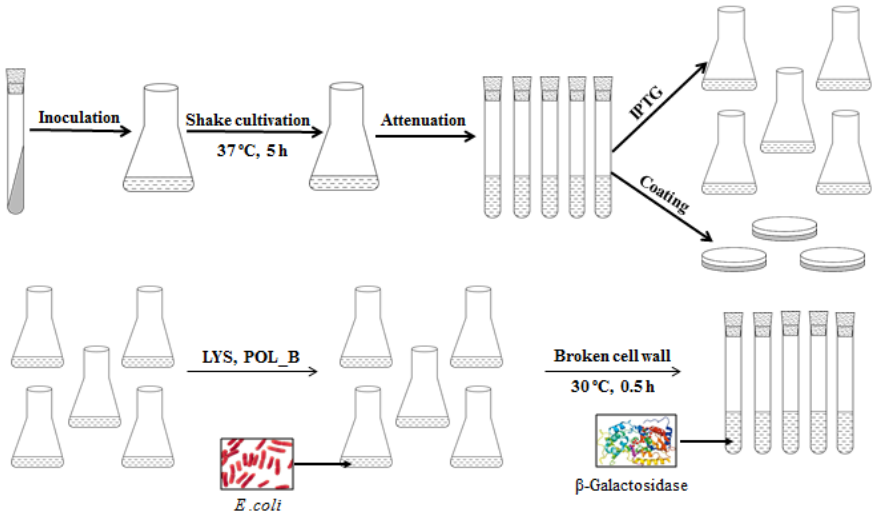

Scheme 2. Cultivation and treatment of *E.coli* as well as the release of β-Gal.

2.4 Preparation of BP/Pt-Pd nanohybrid

The GCE (3mm in diameter) was first mechanically polished with alumina paste (0.3 μm), and rinsed with doubly distilled water, and then further cleaned ultrasonically in 1.0 M HNO_3, 1.0 M NaOH, acetone and doubly distilled water successively. After cleaning, 5 μL BP was drop-coated on the GCE surface, and dried in infrared oven. Then, the electrode was performed in supporting electrolyte containing 1.5 mM H_2PtCl_6, 0.7 mM K_2PdCl_6, 0.1 M Na_2SO_4 and 0.1 M H_2SO_4 by scanning between -0.6 and 1.0 V at 50 mV s^{-1} for 14 cycles for surface modification. BP/Pt-Pd/GCE was washed repeatedly with doubly distilled water to remove unwanted residuals.

2.5 Electrochemical measurements

PAP was put into 5 mL PBS buffer (pH 6.0), which was performed using differential pulse voltammetry (DPV) in scanning ranges between -0.1 and 0.5 V to record the peak current response of PAP. β-Gal was added into 2 mM PAPG in 5 ml PBS buffer (pH 6.0), which keep the temperature at 45 ºC with a constant stirring rate to produce PAP. Two minutes later, the solution was scanned using DPV in the same way to record the peak current response of PAP. Then β-Gal was replaced with *E. coli* and the solution was treated in the same way to record the peak current response of PAP.

3. RESULTS AND DISCUSSION

3.1 Surface morphology of BP-supported Pt-Pd nanoelectrocatalyst

The SEM image of BP (Fig.1a) shows that the BP layer on the surface of GCE is a typical flake-like structure, presenting as an inhomogeneous and discontinuous nanosheet structure. The SEM image of bimetallic Pt-Pd nanoparticles decorated BP revealed that inhomogeneous nanoparticles was co-electrodeposited BP nanosheets with large specific surface area [9] (Fig.1b), which increased the contact area between the surface of the modified electrode and the electrolyte, and significantly enhanced the electrocatalytic capacity of the BP modified electrode.

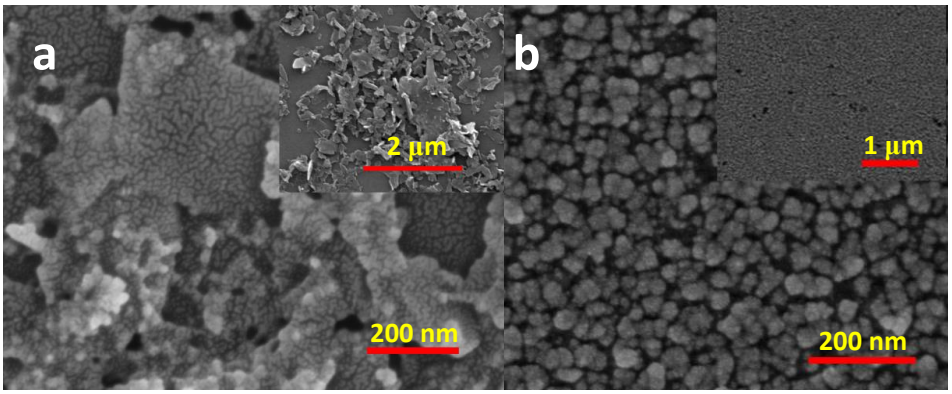

Figure 1. Different magnification SEM images of BP (a) and BP-Pt/Pd (b)

3.2 Electrochemical properties of BP-supported Pt-Pd nanoelectrocatalyst

3.2.1 Electrode stability

The ambient stability of the Pt-Pd/BP/GCE was assessed by the continuous CV method (Fig. 2a). Ninety successive measurements in $[Fe(CN)_6]^{3-/4-}$ were recorded with the relative standard deviation (RSD) of 2.45% (anodic peak) and 2.67% (cathodic peak), indicating that Pt-Pd/BP/GCE had no significant loss of electroactivity in an aqueous solution containing oxygen, suggesting that the Pt-Pd/BP/GCE was good ambient electrode stability (the bare pure BP fast converted to oxides (P_xO_y) in the presence of water containing oxygen and further decomposed into acids or salts within minutes, which seriously impeded electrochemical applications due to the loss of electroactivity [34, 35]) because the surface of BP nanosheets was covered/encased by electrochemical co-deposition of bimetallic Pt-Pd.

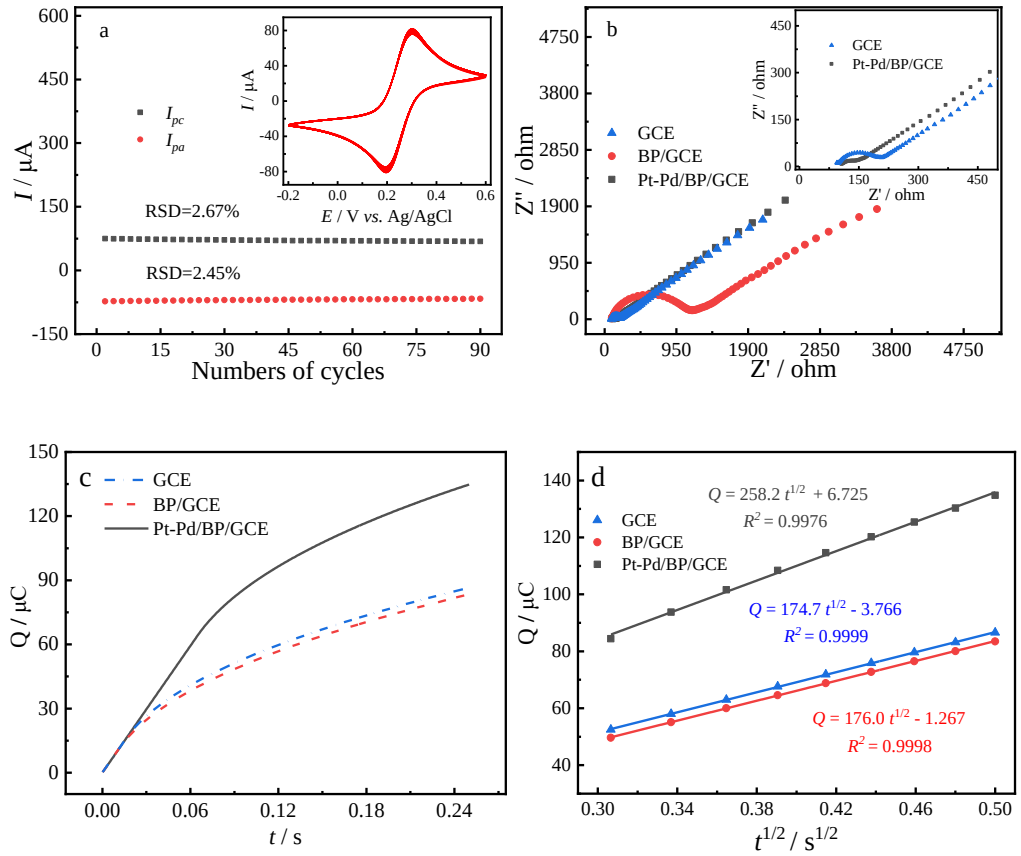

Figure 2. Electrochemical stability (a) of CVs with 90 cycles of Pt-Pd/BP/GCE and Nyquist plots (b) of different electrodes in 5 mM $[Fe(CN)_6]^{3-/4-}$ containing 0.1 M KCl. Q - t curves (c) and $Q - t^{1/2}$ (d) curve of different electrodes in 5 mM $[Fe(CN)_6]^{3-/4-}$ containing 0.1 M KCl.

3.2.2 Electron transfer resistance

Interface characteristics of different modified electrodes were characterized by electrochemical impedance spectroscopy (EIS). The semicircle diameter in the nyquist plot of impedance spectra corresponds to the electron transfer resistance (R_{ct}) of the electrode surface. As shown in Fig. 2b, the R_{ct} of BP modified electrode was much higher than bare electrode, because the BP hindered the transfer of the electrode surface charge due to the poor conductivity. Nevertheless, the R_{ct} of Pt-Pd/BP/GCE rapidly declined, indicating that the bimetallic Pt-Pd nanoparticles improved the conductive path between the electrode and the electrolyte and enhanced the diffusion of $[Fe(CN)_6]^{3-/4-}$ to the electrode surface.

3.2.3 Electrochemical effective area

Large specific surface area can provide a large adsorption capacity, which is conducive to the full contact between the electrode material and electrolyte, reduce the detection limit and improve the sensitivity of the sensor. The effective surface areas of different modified electrodes were measured in 5 mM $[Fe(CN)_6]^{3-/4-}$ by chronocoulometry (Fig. 2c). According to the Anson equation [36]:

$$Q(t) = \frac{2nFAcD^{\frac{1}{2}}t^{\frac{1}{2}}}{\pi^{\frac{1}{2}}} + Q_{dl} + Q_{ads}$$

where A is the effective surface area, c is the concentration of substrate, D is diffusion coefficient, n is the electron number, Q_{dl} is double layer charge which could be eliminated by background subtraction and Q_{ads} is Faradic charge, F, π have their usually meanings. For $[Fe(CN)_6]^{3-/4-}$, the D is 7.6×10^{-6} cm^2 s^{-1}, n is 1. The linear equation of Q *vs* $t^{1/2}$ curves in different electrodes were shown in Fig. 2d. The electroactive surface area of Pt-Pd/BP/GCE (A = 0.086 cm^2) was significantly increased compared with that of the bare electrode (A = 0.059 cm^2) due to BP with the large specific surface area.

3.3 Sensing application of BP-supported Pt-Pd nanoelectrocatalyst

3.3.1 Voltammetric behaviors of PAP

The voltammetric behaviors (Fig. 3) of PAP were investigated using bare GCE, BP/GCE, Pt/BP/GCE, and Pt-Pd/BP/GCE by DPV in scanning potential ranges between - 0.1 and + 0.5 V, respectively. An obvious oxidation peak (0.17 V *vs.* Ag/AgCl) of PAP was observed at the bare GCE (Fig. 3a). While the peak current of PAP observably increased when BP was modified onto GCE (Fig. 3b), which were ascribed to large electrochemical active area of BP for the electrocatalytic oxidation of PAP [37]. The peak current of PAP (Fig. 3c) observably increased when Pt was modified onto GCE, which was assigned to the outstanding electrocatalytic ability of noble metal nanomaterials, Pt-Pd/BP/GCE displayed the best peak current response of PAP (Fig. 3d), indicating that the bimetallic Pt-Pd nanoparticles decorated BP has more superior electrocatalytic activity due to the synergistic effect among two noble metal nanoparticles, and current signals of a bimetallic system were larger and

more stable than that of monometallic system, which was in accordance with literature [38].

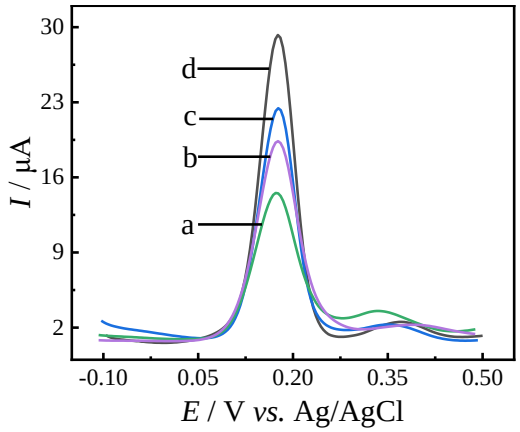

Figure 3. Corresponding DPVs of PAP with GCE (a), BP/GCE (b), Pt/BP/GCE (c), Pt-Pd/BP/GCE (d).

3.3.2 Optimization of sensing parameters

The effects of scan rates (v) on voltammetric responses of PAP using Pt-Pd/BP/GCE were investigated by cyclic voltammetry (CV, Fig. 4). A pair of well-defined oxidation-reduction peak of PAP and the ratios of the oxidation-reduction peak currents are approximately 1, indicating that a good reversible electron transfer process for the redox reaction of PAP using Pt-Pd/BP/GCE. Fig. 4b shows that peak heights of PAP produced linear relationship with the square root of scan rates ($v^{1/2}$), suggesting that the electron transfer process for Pt-Pd/BP/GCE was a typically diffusion controlled. Fig. 4c shows that the linear equations between oxidation/reduction peak potential and the logarithm of sweep speed. According to Laviron theory, the electron-transfer coefficient (α) and electron-transfer number (n) were estimated by using following equations:

$$E_{pa} = E^0 + \frac{RT}{\alpha nF}\ln\left(\frac{RTks}{\alpha nF}\right) - \frac{RT}{\alpha nF}\ln v$$

$$E_{pc} = E^0 + \frac{RT}{(1-\alpha)nF}\ln\left[\frac{RTks}{(1-\alpha)nF}\right] - \frac{RT}{(1-\alpha)nF}\ln v$$

Where α is the charge transfer coefficient, R, T and F have their conventional meanings (R = 8.314 J mol^{-1} K^{-1}, T = 298 K, and F = 96485 C mol^{-1}). The α and n values were found to be 0.69 and 2, respectively.

The effect of pH on electrochemical responses of PAP at Pt-Pd/BP/GCE within ranges from 3 to 9 was investigated by CV. The relationship between the redox peak height and pH values were presented in Fig. 5a. Results showed that the redox peak height of PAP increased with the increasing pH until the highest peak height. The peak current of oxidation reaches the maximum value at pH 6, then markedly decreased with the increase of pH, while the peak current of reduction reached the maximum value at pH 7.5, so 6.0 was regarded as the optimal pH value. In addition, the relationship between the redox peak potentials (E) and pH values were demonstrated in Fig. 5b.

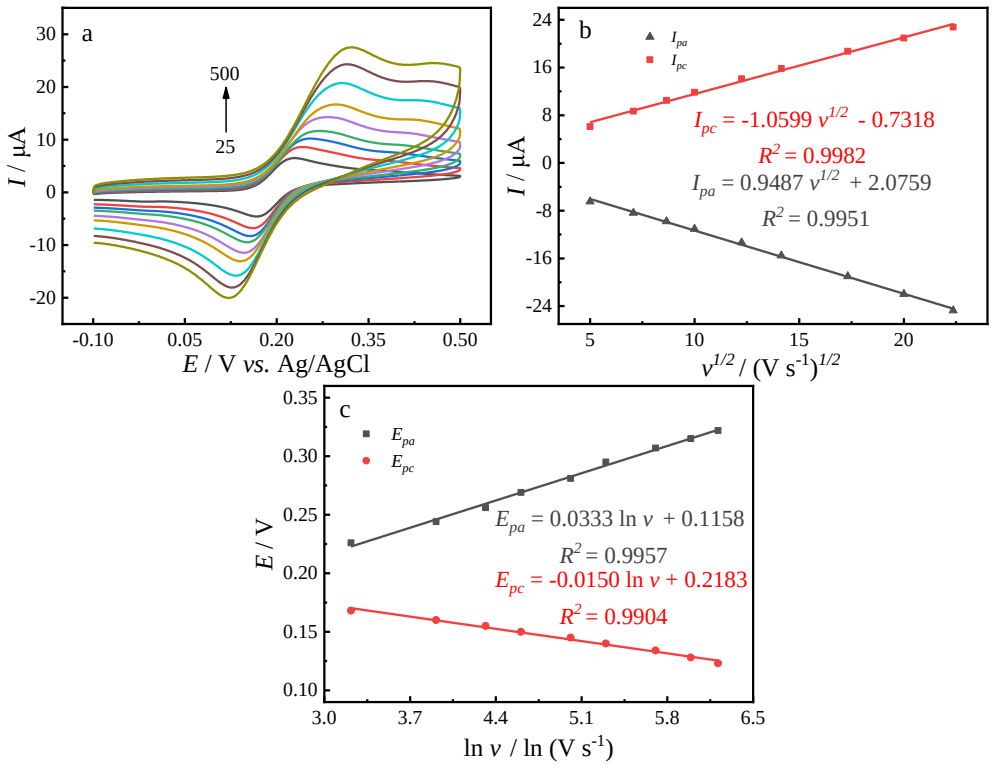

Figure 4. Corresponding CVs of the response current of 0.4 mM PAP with different scan rates (25, 50, 75, 100, 150, 200, 300, 400, 500 mV/s) (a); The linear relation between the peak current of 0.4 mM PAP and the $v^{1/2}$ (b); The linear relation between the peak potential of 0.4 mM PAP and ln v (c).

The oxidation/reduction peak potentials shifted negatively and increased linearly with the increasing pH values, indicating that the proton took part in oxidation process of the electrode.

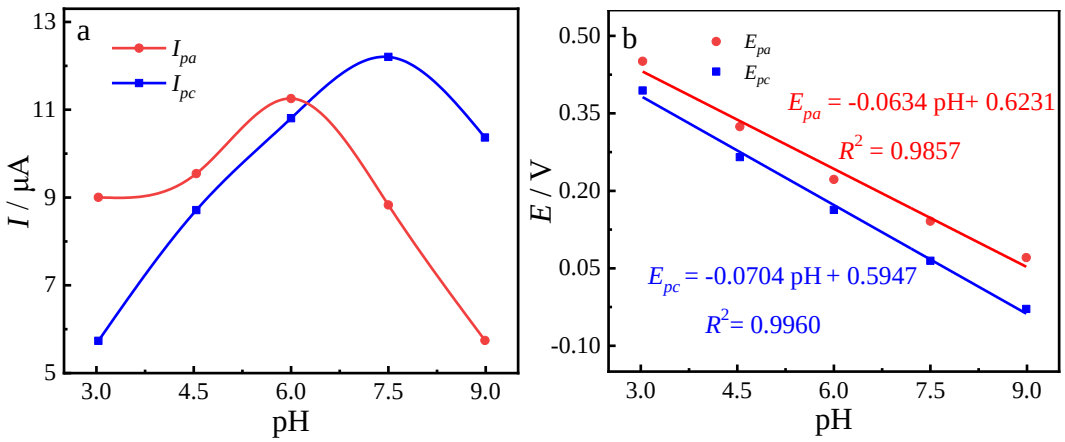

Figure 5. Effect of pH on the peak current (a) and peak potential (b) for the oxidation and reduction of 0.4 mM PAP.

According to the Nernst equation, the slopes of two equations are close to the theoretical value of 0.059 V pH^{-1}, proving that the number of protons and electrons involved in the electrode reaction

are equal. Therefore, the number of protons was concluded as 2, implying that the number of both electron and proton was equal. Thus, the electrochemical redox of PAP was a two-electron and two-proton process, the electrochemical reaction mechanism of PAP was presented in Scheme 3.

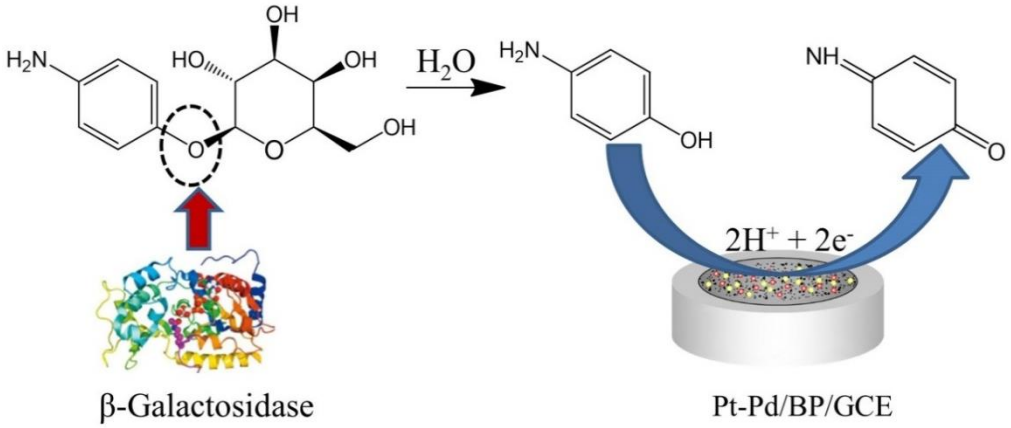

Scheme 3. The enzyme-catalytic reaction of PAPG via β-Gal and its electrocatalytic reaction on the surface of Pt-Pd/BP/GCE.

3.3.3 Biochemical reaction of PAPG and its voltammetric behaviors

PAP as an electroactive product was obtained by the hydrolysis of PAP-β-D-galactopyranoside (PAPG) using β-Gal that was produced by coliforms or *E. coli* that are induced by isopropyl-β-D-thiogalactopyranoside (IPTG).

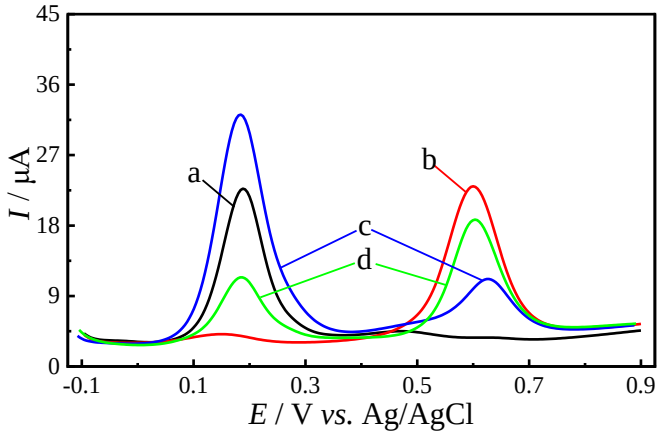

Figure 6. Corresponding DPVs of PAP (a), PAPG (b), PAPG + β-Gal (c) and PAPG + *E. coli* (d).

The voltammetric behaviors (Fig. 6) of PAP (a), PAPG (b), PAPG + β-Gal (c) and PAPG + *E. coli* (d) were investigated using DPV in scanning potential ranges between - 0.1 and + 0.9 V, respectively. An oxidation peak was observed in PBS containing PAP using Pt-Pd/BP/GCE, while another oxidation peak was observed in PBS containing PAPG using Pt-Pd/BP/GCE. Obviously, two oxidation peaks were observed in PBS containing PAPG + β-Gal or PAPG + *E. coli*. Namely, two oxidation peaks were peaks of both PAP and PAPG that was produced in the presence of PAPG + β-

Gal or PAPG + *E. coli* (Fig. 6).

3.3.4 Activation energy of β-Gal

The bioactivity of β-Gal strongly depends on the temperature, which may inactivate at very high or low temperature. The effect of temperature on the relative bioactivity of the β-Gal was tested by DPV. The maximum of current response was obtained at 318 K (Fig. 7a and b).

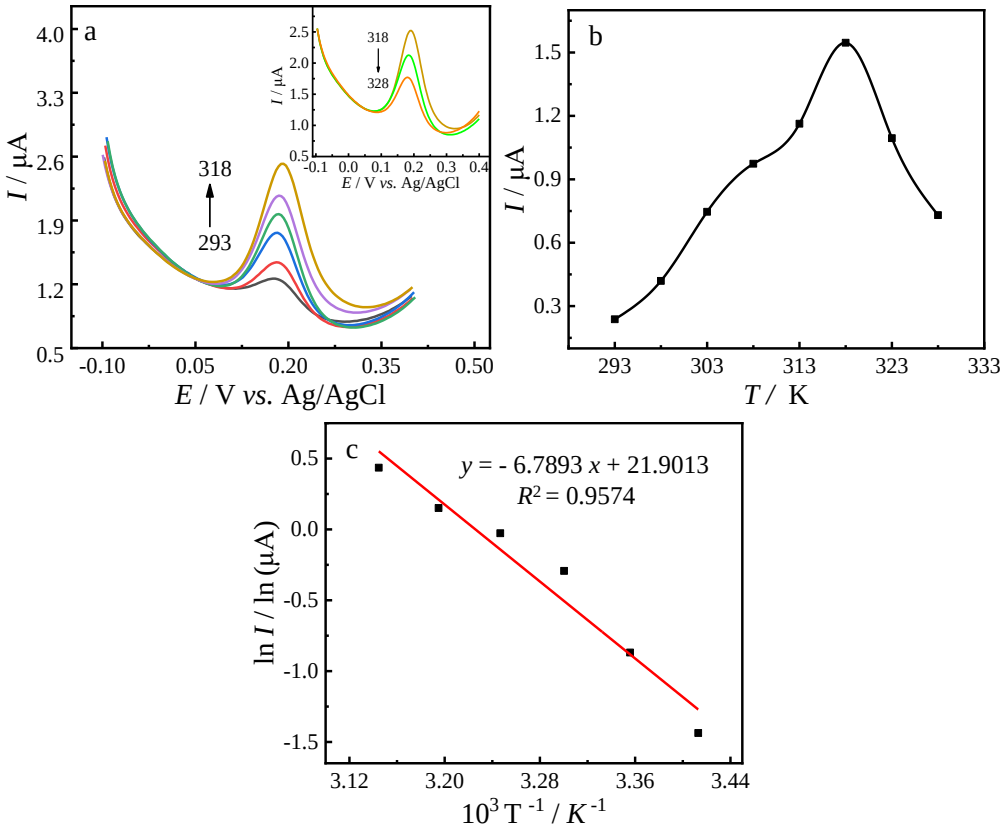

Figure 7. (a) Corresponding DPVs of β-Gal at different temperature (293-318 K). Inset: Corresponding DPVs of β-Gal at different temperature (318-328 K). (b) The curves of β-Gal's response current at different temperature. (c) The determination of apparent activation energy.

In addition, the activation energy (E_a) was assessed by the bioactivity and affinity of enzyme for substrate [35] that was obtained by ln *I vs.* T^{-1} graphs (Fig. 7c). The ln *I vs.* T^{-1} graphs depicts the linear relationship between the napierian logarithm of *I* and the inverse of the temperature. The value of E_a was calculated by the Arrhenius equation as follows:

$$\ln k = \ln k_0 - \frac{E_a}{RT} \Rightarrow \ln I = \ln I_0 - \frac{E_a}{RT}$$

Here, *I* is the peak current, I_0 is a collection of currents, *R* is the universal gas constant, and *T* is the absolute temperature in Kelvin. After linear regression, an equation was obtained. $-E_a$/R was

obtained from the slope according to the Arrhenius equation, thus the E_a was 56.45 kJ M^{-1}.

3.4 Sensing performance

The analytical performance of the developed nanohybrid sensor was investigated by DPV under the optimal conditions (Fig. 8). Fig. 8a and d shows that the peak height increased linearly with increases of PAP concentrations in ranges from 2 × 10^{-8} to 5 × 10^{-6} M, and the corresponding linear regression equation can be expressed as I_{pa} (μA) = 9.9564 C + 1.2227 (μM) (R^2 = 0.9911), and the limit of detection (LOD) was defined as 3s/k, Sensitivity = k/A, where k is the slope of the linear calibration line and s is the standard deviation of replicate determination values under the same conditions as for the sample analysis in the absence of analytes [39]. In this work, the Pt-Pd/BP/GCE was measured repeatedly for 10 times in blank solution to estimate the standard deviation (s). So, the value calculated for LOD is 1.41 × 10^{-8} M and a sensitivity of 115.81 μA·μM^{-1}·cm^{-2}. This study provides a lower detection limit than previously reported electrochemical sensor detection of PAP (Table 1).

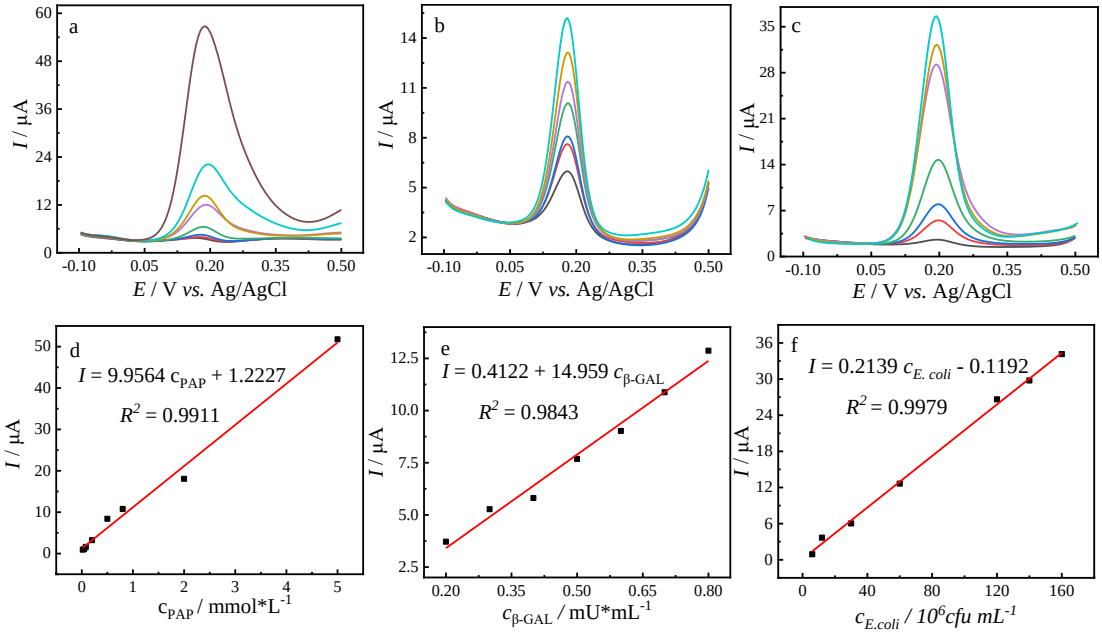

Figure 8. Corresponding DPVs of different PAP concentration (a), different β-Gal concentration (b), and different *E.coli* concentration (c); The linear relation between PAP concentration and response current size (d), β-Gal concentration and response current size (e), *E.coli* concentration and response current size (f).

Similarly, peak height was proportional to increases of β-Gal concentrations in ranges from 0.2 - 0.8 mU·L^{-1} (Fig. 8b and e), and the corresponding linear regression equation can be expressed as I_{pa} (μA) = 14.959 C + 0.4122 (mU) (R^2 = 0.9843), Moreover, the proposed sensor has a LOD of 9.35 nU·L^{-1} and a sensitivity of 4.77 μA (mU·L^{-1})$^{-1}$·cm^{-2}. The Pt-Pd/BP/GCE showed a great linear range

from from 6×10^6 to 1.6×10^8 cfu·mL^{-1} (Fig. 8c and f), and the corresponding linear regression equation was I_{pa} (μA) = 9.9564 C + 1.2227 (cfu·mL^{-1}) (R^2 = 0.9911) with LOD of 6.65×10^5 cfu·mL^{-1} and a sensitivity of 2.44 μA·(cfu·mL^{-1})$^{-1}$·cm^{-2}. Compared with previously reported sensors based on enzyme for the voltammetric detection of *E. coli,* the fabricated sensor shows new ideas for faster detection of *E. coli* by voltammetry (Table 2).

Table 1 Comparison of various electrodes for electrochemical determination of PAP.

Electrode	detection object	LOD (M)	Linear range (μM)	Reference
Molecularly Imprinted Polymer/hemin-graphene/GCE	PAP	6×10^{-8}	0.3~25 μM	[40]
Single-wall carbon nanotubes/poly(4-aminopyridine)/GCE	PAP	6×10^{-8}	0.2–100μM	[41]
Graphene-Nafion/GCE	PAP	5.1×10^{-8}	0.5–200	[42]
aPcCo-CNTb[a]/GCE	PAP	3×10^{-7}	0.5–800	[43]
Pt-Pd/BP/GCE	PAP	1.41×10^{-8}	0.02- 5μM	This study

[a]The hybrid of tetra-β-[3-(dimethylamine)phenoxy] phthalocyanine cobalt(II) and acid-treated 10 multiwalled carbon nanotube.

Table 2 The comparison of the fabricated sensor with previously reported sensors based on enzyme for the voltammetric detection of *E. coli.*

Tec.	Signal molecule	Working potential	Tem. (ºC)	pH	Reaction time	Liner range	LOD (cfu/mL)	Ref.
CV	PAP	0.1 ~ 0.5 V	42	6.8	3 h	5×10^4 - 10^8	-	[44]
I-t	PAP	0.3 V	44.5	7.3	-	-	-	[45]
I-t	*o*-Nitrophenyl	0.93 V	50	7	-	4×10^4 - 6×10^6	4×10^4	[46]
DPV	PAP	-0.1~0.5V	45	6	5 min	6×10^6 - 1.6×10^8	6.65×10^5	This study

4. CONCLUSION

The BP-supported Pt-Pd nanoelectrocatalyst as multifunctional chemo/biosensing platform for voltammetric detection of PAP, β-Gal, and Escherichia *E. coli* was successfully fabricated by the electrodeposition of bimetallic Pt-Pd nanoparticles onto the BP surface. The BP-supported Pt-Pd nanoelectrocatalyst displayed ambient stability in aqueous buffer containing oxygen, high electron transfer resistance, large electrochemical active area, remarkable voltammetric responses for PAP in a linear range of 0.02 - 5 μmol·L^{-1} with a detection limit (LOD) of 1.41×10^{-8} M and sensitivity 115.81 μA·μM^{-1}·cm^{-2}. PAP could obtain though the biochemical reaction of β-Gal in the presence of substrate PAP-β-galactopyranoside, which could realize for biochemical sensing of β-Gal in a linear range of 0.2 - 0.8 mU·L^{-1} with a LOD of 9.35 nU·L^{-1} and sensitivity of 4.77 μA (mU·L^{-1})$^{-1}$·cm^{-2}. The β-Gal is an indicator of total coliforms represented by *E. coli* that are induced by isopropyl-β-thiogalactopyranoside, which could applied for biochemical sensing of *E. coli* in a linear range of 6 ×

$10^6 – 1.6 \times 10^8$ cfu·mL^{-1} with LOD of 6.65×10^5 cfu·mL^{-1} and sensitivity of 2.44 μA·(cfu·mL^{-1})$^{-1}$·cm^{-2} and it was very necessary for further research on the improvement of sensitivity of *E. coli* sensing.

ACKNOWLEDGEMENT
This work was supported by the National Natural Science Foundation of China (51662014, 51962007, 51762020), the Outstanding Young Talent Program of Jiangxi Province (20171BCB23042), the Academic and Technical Leader Plan of Jiangxi Provincial Main Disciplines (20182BCB22014) and Youth Key Project of Natural Science Foundation of Jiangxi Province (20192ACBL21015).

References

1. L. Li, Y. Yu, G. J. Ye, Q. Ge, X. Ou, H. Wu, Y. Zhang, *Nat. Nanotechnol.,* 9 (2014) 372.
2. P. Chen, N. Li, X. Chen, W. J. Ong, X. Zhao, *2D Mater.,* 5 (2017) 014002.
3. Y. Abate, D. Akinwande, S. Gamage, H. Wang, M. Snure, N. Poudel, S. B. Cronin, *Adv. Mater.,* 30 (2018) 1704749.
4. X. Niu, W. Weng, C. Yin, Y. Niu, G. Li, R. Dong, Y. Men, W. Sun, *J. Electroanal. Chem.*, 811 (2018) 78.
5. H. Ding, L. Zhang, Z. Tang, Y. Dong, X. Chu, *J. Electroanal. Chem.*, 824 (2018) 161.
6. J. Cai, B. Sun, W. Li, X. Gou, Y. Gou, D. F. Li, *J. Electroanal. Chem.*, 835 (2019) 1.
7. Z. Zhang, Y. Li, J. Xu, Y. Wen, J. Electroanal. Chem., 814 (2018) 153.
8. Y. Xiang, M. B. Camarada, Y. Wen, H. Wu, J. Chen, M. Li, X. Liao, *Electrochim. Acta,* 282 (2018) 490.
9. Y. Ge, M. B. Camarada, L. Xu, M. Qu, H. Liang, E. Zhao Y. Wen, *Microchim. Acta,* 185 (2018) 566.
10. Y. Ge, M. Qu, L. Xu, X. Wang, J. Xin, X. Liao, M. Li, M. Li, Wen, Y. *Microchim. Acta,* 186 (2019) 836.
11. T. Xue, Y. Sheng, J. Xu, Y. Li, X. Lu, Y. Zhu, X. Duan, Y. Wen, *Biosens. Bioelectron.,* 145 (2019) 111716.
12. C. M. Welch, R. G. Compton, *Anal. Bioanal. Chem.,* 384 (2006) 601.
13. C. H. Liu, R. H. Liu, Q. J. Sun, J. B. Chang, X. Gao, Y. Liu, S. T. Lee, Z. H. Kang, S. D. *Nanoscale,* 7 (2015) 6356.
14. W. Yu, M. D. Porosoff, J. G. Chen, *Chem. Rev.,* 112 (2012) 5780.
15. H. Liu, R. Fang, Z. Li, Y. Li, *Chem. Eng. Sci.,* 122 (2015) 350.
16. H. Zhang, M. Jin, Y. Xia, *Chem. Soc. Rev.,* 41 (2012) 8035.
17. G. Sharma, A. Kumar, S. Sharma, M. Naushad, D R. P. wivedi, Z. A. ALOthman, G. T. Mola, *J. King Saud U. Sci.,* 31 (2019) 257.
18. C. H. Liu, R. H. Liu, Q. J. Sun, J. B. Chang, X. Gao, Y. Liu, S. D. Wang, *Nanoscale,* 7 (2015) 6356.
19. B. Yoon, C. M. Wai, *J. Am. Chem. Soc.,* 127 (2005) 17174.
20. G. G. Wildgoose, C. E. Banks, R. G. Compton, *Small,* 2 (2006) 182.
21. O. Clermont, S. Bonacorsi, E. Bingen, *Appl. Environ. Microbiol.,* 66 (2000) 4555.
22. M. A. Croxen, R. J. Law, R. Scholz, K. M. Keeney, M. Wlodarska, B. B. Finlay, *Clin. Microbiol. Rev.,* 26 (2013) 822.
23. N. Tawil, E. Sacher, R. Mandeville, M. Meunier, *Biosens. Bioelectron.,* 37 (2012) 24.
24. M. B. Dos Santos, J. P. Agusil, B. Prieto-Simón, C. Sporer, V. Teixeira, J. Samitier, *Biosens. Bioelectron.,* 45 (2013) 174.
25. X. Jiang, K. Chen, J. Wang, K. Shao, T. Fu, F. Shao, H. Han, *Analyst,* 138 (2013) 3388.
26. W. C. Liao J. A. Ho, *Anal. Chem.,* 81 (2009) 2470.

27. J. Chen, Z. Jiang, J. D. Ackerman, M. Yazdani, S. Hou, S. R. Nugen, V. M. Rotello, *Analyst*, 140 2015 4991.
28. M. Zhong, L. Yang, H. Yang, C. Cheng, W. Deng, Y. Tan, S. Yao, *Biosens. Bioelectron.*, 126 (2019) 493.
29. Y. W. Zhao, H. X. Wang, G. C. Jia, Z. Li, *Sensors*, 18 (2018) 2518.
30. E. B. Setterington, E. C. Alocilja, *Biosens. Bioelectron.*, 26 (2011) 2208.
31. X. Zhang, P. Geng, H. Liu, Y. Teng, Y. Liu, Q. Wang, L. Jiang, *Biosens. Bioelectron.*, 24 (2009) 2155.
32. X. Zhang, J. Shen, H. Ma, Y. Jiang, C. Huang, E. Han, Y. He, *Biosens. Bioelectron.*, 80 (2016) 666.
33. Y. Li, J. Deng, L. Fang, K. Yu, H. Huang, L. Jiang, J. Zheng, *Biosens. Bioelectron.*, 63 (2015) 1.
34. J. Zhang, W. Ding, Z. Zhang, J. Xu, Y. Wen, *RSC Adv.*, 6 (2016) 76174.
35. Y. Abate, D. Akinwande, S. Gamage, H. Wang, M. Snure, N. Poudel, S. B. Cronin, *Adv. Mater.*, 30 (2018) 1704749.
36. J. Chang, W. Xiao, P. Liu, X. Liao, Y. Wen, L. Bai, M. Li, *J. Electroanal. Chem.*, 780 (2016) 103.
37. V. Selvaraj, M. Alagar, I. Hamerton. *J. Power Sources*, 160 (2006) 940.
38. Y. Wen, J. Xu, M. Liu, D. Li, L. Lu, R. Yue, H. He, *J. Electroanal. Chem.*, 674 (2012) 71.
39. D. R. Thévenot, K. Toth, R. A. Durst, G. S. Wilson, *Anal. Lett.*, 34 (2001) 635.
40. Y. Liu, K. Yan, B. Wang, C. Yang, J. Zhang, *J. Electrochem. Soc.*, 164 (2017) B776-B780.
41. Z. Wang, H. Zhu, H. Zhang, G. Gao, Z. Sun, H. Liu, X. Zhao, *Electrochim. Acta*, 54 (2009) 7531-7535.
42. Filik, H., Çetintaş, G., Koç, S. N., Gülce, H., & Boz, İ. (2014). *Russ. J. Electrochem.,* 50243-252.
43. L. Guo, Z. Chen, J. Zhang, H. Wu, F. Wu, C. He, B. Wang Y. Wu, *RSC Adv.,* 5 (2015) 23283-23290.
44. M. Rochelet, S. Solanas, L. Betelli, B. Chantemesse, F. Vienney, A. Hartmann, *Anal. Chim. Acta* 892 (2015) 160-166.
45. F. Pérez, I. Tryland, M. Mascini, L. Fiksdal, *Anal. Chim. Acta* 427 (2001) 149-154.
46. E. Majid, K. B. Male, J. H. Luong, *J. Agric. Food Chem.* 56 (2008) 7691-7695.